

DeepCSHAP: Utilizing Shapley Values to Explain Deep Complex-Valued Neural Networks

Florian Eilers¹ and Xiaoyi Jiang¹

Department of Computer Science, University of Münster, Germany
{florian.eilers,xjiang}@uni-heidelberg.de

Abstract. Deep Neural Networks are widely used in academy as well as corporate and public applications, including safety critical applications such as health care and autonomous driving. The ability to explain their output is critical for safety reasons as well as acceptance among applicants. A multitude of methods have been proposed to explain real-valued neural networks. Recently, complex-valued neural networks have emerged as a new class of neural networks dealing with complex-valued input data without the necessity of projecting them onto \mathbb{R}^2 . This brings up the need to develop explanation algorithms for this kind of neural networks. In this paper we provide these developments. While we focus on adapting the widely used DeepSHAP algorithm to the complex domain, we also present versions of four gradient based explanation methods suitable for use in complex-valued neural networks. We evaluate the explanation quality of all presented algorithms and provide all of them as an open source library adaptable to most recent complex-valued neural network architectures.

Keywords: Explainable AI · Complex-valued Neural Networks

1 Introduction

Many applications profit from the success of deep neural networks. Most applications deal with real-valued numbers, such as natural images, encodings for natural language or real-valued signals. The standard real-valued deep neural networks are suitable to solve problems with these kinds of data. There is a class of applications, however, that naturally deal with complex numbers in the data, such as MRI [8], PolSAR satellite images [4] or Fourier transforms of real-valued signals for frequency analysis [29]. These kinds of data motivate the use of complex-valued neural networks (CVNNs), where all building blocks of deep neural networks are translated to the complex domain to directly process these data without use of an isomorphism from \mathbb{C} to \mathbb{R}^2 . It has been shown that in many applications (but not all [32]) complex-valued neural networks show superior performance, especially when dealing with complex-valued input data but sometimes even when dealing with real-valued input data [15].

On major drawback of real- and complex-valued deep learning architectures is their lack of interpretation. Their (often) millions of parameters make them

hard to understand and interpret, leading to the often referred to black box. To (partially) solve this issue, many methods in the regime of explainable artificial intelligence (XAI) have been proposed for real-valued neural networks. Early works in this regime work with explanations based on gradients [24, 25, 27] while more recent works make use of more sophisticated methods, such as local linearization of the model [22, 23] or Shapley values - a measure for cooperative games from game theory [26].

To the best of our knowledge, no explanation methods have been proposed to explain complex-valued neural networks. Directly applying real-valued explanation algorithms to complex-valued architectures is often impossible and the adaptations are non trivial. In this paper, we aim to fill this gap by developing a complex-valued variant of the widely used DeepSHAP [20] algorithm. We provide proofs for the complex-valued chain rule used within the algorithm as well as for some desirable properties that reduce computational complexity. Additionally, we adapt four gradient based explanation methods to the complex domain. We then evaluate explanation quality of all of these methods on two datasets - one real-valued and one complex-valued dataset. Additionally, we validate our theoretical findings on these two datasets.

The key contributions of our work are:

1. Development of a complex-valued DeepSHAP algorithm, including the proof of a complex-valued chain rule.
2. Adaptation of four gradient based explanation methods to the complex domain.
3. Evaluation of explanation quality of these five methods on two complex-valued neural networks applied to a real-valued and a complex-valued dataset.
4. Validation of theoretical results on these two datasets.

The source code with a pytorch library containing all the explanation methods in section 4 and section 5, as well as all experiments from section 6 is publicly available¹.

2 Related work

2.1 Explanation methods

Early explanation methods are mostly based on gradients. Simonyan et al. [24] use gradients as an explanation method. This idea is then extended to Guided Backpropagation [25], where negative gradients are zeroed out throughout the backward pass. Sundararajan et al. [27] propose the integrated gradients methods, where instead of using the plain gradients, they integrate the gradients over an interpolation from a starting value (e.g. an all zeros image) to the actual image. Lastly, Bach et al. propose Layerwise Relevance Propagation [3], which is not a gradient based method per se, but is equivalent to computing the gradient times the input under certain assumptions [13].

¹ In the supplementary material for reviewers, online after publication.

LIME by Riberiro et al. [22] aims to locally explain a model’s output by fitting a linear model in a neighborhood of a certain input. This local linear model is easily explainable and is used to locally explain the more complex model.

DeepLIFT by Shrikumar et al. [23] introduces an explanation method that only needs one backward pass to explain a model output for a specific input. They define heuristic rules how to explain single layers and then define a chain rule on how to explain a full network as a concatenation of these layers.

SHAP [20] is a framework that defines a class of explanation methods - additive feature attribution methods - by an additive property, which is already satisfied by LIME and DeepLIFT. They formulate three axioms based on Shapley values from game theory and show that their defined SHAP values is the only explanation method to fulfill all of those axioms. They then derive kernelSHAP, a combination of Linear LIME and Shapley values as well as DeepSHAP, which makes use of the chain rule from DeepLIFT but replaces the heuristic rules with SHAP values for every layer. A complex-valued adaptation of DeepSHAP is the main focus of this work, so DeepSHAP will be explained in detail in subsection 3.2. Many variants of these methods have been proposed and are widely used in the literature [1].

2.2 Complex-valued neural networks

After early works by Hirose et al. [11], the main building blocks for complex-valued convolutional neural networks have been explored by Trabelsi et al. [29]. More recently there have also been developments of a complex-valued transformer architecture [9, 31] and many more architectures [17]. In the last two years, besides numerous applications, there have been multiple theoretical works on complex-valued neural networks, such as analysis of training behavior [28] and the ability to generalize [6] as well as hardware optimizations for complex-valued calculations [33]. A multitude of complex-valued architectures have been used for applications such as MRI reconstruction [8, 30], PolSAR image processing [4, 18], speech enhancement [7, 12]. A broad overview over the field can be found in [5, 17].

To the best of our knowledge, there exist no works on explainability complex-valued neural networks. Mayer et al. [21] mention that they are not able to explain their model, since SHAP in its current form is not suitable for complex-valued neural networks. There are works that use explainability methods for real-valued neural networks to process complex-valued data [19], which is a different approach that does not benefit from the success of complex-valued neural networks and is thus out of scope of this paper.

3 Real-valued explanation methods

3.1 Gradient based methods

A straightforward method for model explanation is to use the gradient of the output w.r.t to the input pixels as an explanation as proposed in [24]. This

can be modified to integrated gradients, where the input image is interpolated from some starting value (e.g. a black/all zeros image) and the gradients of all interpolation steps are integrated [27]. Additionally, by multiplying the gradients with the input image an approximation of Layerwise Relevance Propagation [3] can be computed, as shown by Kindermans et al. [13].

Lastly Guided Backpropagation [25] uses gradients as an explanation but zeros out negative gradients (i.e. applies ReLU on the gradients) throughout the backward pass.

3.2 DeepSHAP

Lundberg et al. [20] define a class of explanation methods - additive feature attribution methods - as explanation models that fulfill Equation 1. For some fixed input x , let f_x be a (local) explanation model, which is a simplified version of the original model that acts on a simplified binary model input defined by a local mapping $h_x(z') = z$ while assuring $f_x(z') \approx f(h_x(z'))$ if $z' \approx x'$. An additive feature attribution method is then defined as a model fulfilling the equation:

$$f_x(z') = \phi_0 + \sum_{j=1}^n \phi_j z'_j \quad (1)$$

Here z' is a binary variable describing the presence or absence of features of the simplified input. They show that multiple methods from the literature [3, 22, 23, 26] already fulfill this definition. They then define a set of desirable axioms for additive feature attribution methods inspired by Shapley values:

Local Accuracy describes the ability of the explanation model to be accurate when evaluated at the target data point. For a model f and its explanation model f_x it should hold that: $f(x) = f_x(x')$.

Missingness describes that the contribution of a feature that is already missing in the simplified input x' , should be zero: $x_j = 0 \Rightarrow \phi_j = 0$.

Consistency means that if a feature has less impact (or stronger negative impact) on a second model, then on the original model, the contribution assigned to that feature for the second model should be smaller than that of the original model: For a simplified input z' let z'/j be z' modified s.t. $z'_j = 0$. For two models f and f' and their explanation models f_x and f'_x it should hold that:

$$\begin{aligned} f'_x(z') - f'_x(z'/j) &\leq f_x(z') - f_x(z'/j) \text{ for all } z' \in \{0, 1\}^n \\ &\Rightarrow \phi_j(f', x) \leq \phi_j(f, x) \end{aligned} \quad (2)$$

Lundberg et al. [20] show that a unique function delivers the solution to these axioms:

$$\begin{aligned} \phi_j(f, x) &:= \sum_{z' \subset x' \setminus j} G_{Mz'} (f_x(z' \cup j) - f_x(z')) \quad (3) \\ \text{with } G_{Mz'} &:= \frac{|z'|!(M - |z'| - 1)!}{M!} \end{aligned}$$

The solution to this equation yields an additive feature attribution model that the authors call SHapley Additive exPlanations (SHAP). They then define different model specific and agnostic approaches to compute the SHAP values.

We focus now on an approach designed for deep neural networks: DeepSHAP. Since the contributions $\phi_j(g, x)$ are easy to calculate for simple building blocks of neural networks, such as linear layers (e.g. convolutions, fully connected layers or normalization layers) and pointwise activation functions (e.g. ReLU, sigmoid), we just need to calculate the contribution of a full model, which is the concatenation of those layers, from the contributions of the individual layers. For this sake the authors use an idea from DeepLIFT [23]: Propagating Contributions through layers by a custom defined chain rule. For that they define multipliers as contributions relative to the input difference:

$$m_{x_f}^j := \frac{\phi_j(f, x)}{x_j - \mathbb{E}(x_j)} \quad (4)$$

They then define a chain rule for these multipliers to propagate the contributions through the layers, similarly of how gradients are backpropagated from individual layer-gradients to calculate the gradient of the full model. Let $h = f \circ g$ with $g(y) = x \in \mathbb{R}^n$, then the chain rule states:

$$m_{y_h}^k = \sum_{j=1}^n m_{y_{g_j}}^k m_{x_f}^j \quad (5)$$

Applying this chain rule iteratively through all the layers makes it possible to compute the multipliers and then by inverting Equation 4 also the contribution of the full neural network.

4 Complex-valued Gradient based methods

In this section, we describe how to adapt commonly used gradient based methods to the complex domain. Since the adaption is rather straight forward, we do not consider this a key contribution, but want to summarize the adaptations, since - to the best of our knowledge - this has not been done before. Additionally, these methods will provide a baseline for the experiments in section 6 to compare DeepCSHAP which is introduced in section 5. The adaption of all methods from subsection 3.1 can be accomplished with the use of Wirtinger calculus. The Wirtinger derivative for a function $f : \mathbb{C} \rightarrow A$ with $A = \mathbb{C}$ or \mathbb{R} are defined as:

$$\frac{\delta f}{\delta z} := \frac{1}{2} \left(\frac{\delta f}{\delta \mathcal{R}(z)} - i \frac{\delta f}{\delta \mathcal{I}(z)} \right) \quad (6)$$

$$\frac{\delta f}{\delta \bar{z}} := \frac{1}{2} \left(\frac{\delta f}{\delta \mathcal{R}(z)} + i \frac{\delta f}{\delta \mathcal{I}(z)} \right) \quad (7)$$

The Wirtinger derivative w.r.t. the complex conjugate $\frac{\delta f}{\delta \bar{z}}$ has the property of pointing in the direction of the strongest ascend and the magnitude of the

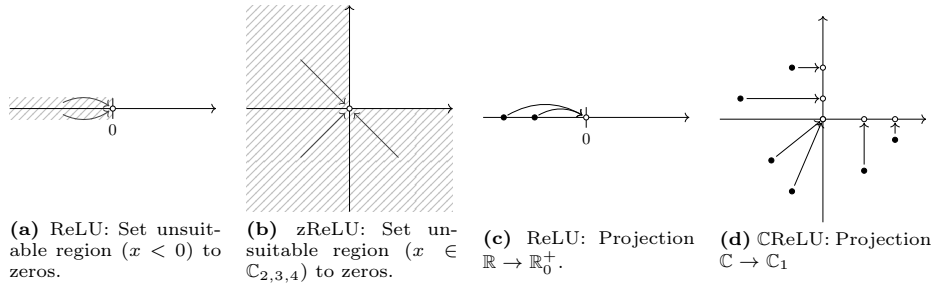


Fig. 1: Two different interpretations of ReLU and their corresponding complex-valued adaptations. \mathbb{C}_n denotes the n -th quadrant.

Wirtinger gradient is equal to the amount of change in that direction [11], just as the gradient does for real-valued functions. Thus, replacing the real-valued gradient in the methods from subsection 3.1 with $\frac{\partial f}{\partial \bar{z}}$ yields explanation methods with a similar interpretation as the methods in subsection 3.1. However, the Wirtinger gradient is complex-valued for complex-valued inputs and is thus not feasible to directly generate a saliency map. The two straight forward options are to take either the magnitude of the complex gradient, or add up its real and imaginary part. The first variant has the drawback of neglecting the sign of the gradient, the second one may show a contribution of zero for non-zero gradients, if the real and imaginary part cancel out. We test both variants in section 6.

To adapt the Guided Backpropagation [25] it is necessary to define an equivalent formulation of "zeroing out negative gradients" in the backward pass for the Wirtinger gradients. There are two different interpretations of the mapping: $ReLU(x) = \max(0, x)$ in the real domain, which lead to different adaptations to the complex domain. The first interpretation is to define a region of unsuitable values (in the real case all negative numbers) and interpret ReLU as the function setting all unsuitable (i.e. negative) values to zero. Secondly, ReLU can be viewed as a projection: \mathbb{R} to \mathbb{R}_0^+ . Thus, every value in \mathbb{R} is mapped to the closest value in \mathbb{R}_0^+ , projecting negative values to zero and positive values to themselves. These interpretations are visualized in Figure 1 a) and c), respectively.

Following the first interpretation we propose to map every input to zero that is not in the first quadrant of \mathbb{C} (i.e. real and imaginary parts are positive), thus defining the quadrants 2-4 as the region of unsuitable values (i.e. the equivalent to negative values in the real case). Following the second of the two interpretations, we propose to project \mathbb{C} to the first quadrant of \mathbb{C} , which yields the function $f(x) = \max(0, \mathcal{R}(x)) + i \max(0, \mathcal{I}(x))$. Both variants are visualized in Figure 1 b) and d), respectively. The resulting formulations for complex-valued ReLU variants are in line with the ReLU variants for deep complex networks as proposed by Trabelsi et al. [29], thus we call these variants Guided z -Backpropagation and Guided \mathbb{C} -Backpropagation, respectively.

5 DeepCSHAP

This section marks the main contribution of this work. We aim to make DeepSHAP applicable to complex-valued neural networks since it is not applicable to complex-valued neural networks, due to its chain rule based on real-valued multipliers, as explained in subsection 5.2.

5.1 CSHAP values

The first question that arises is how to define SHAP values in the complex-valued context, which is possible by simply adopting the definition from Equation 3:

$$\phi_j(f, x) := \sum_{z' \subset x' \setminus j} G_{Mz'} (f_x(z' \cup j) - f_x(z')) \quad (8)$$

with $G_{Mz'} := \frac{|z'|!(M - |z'| - 1)!}{M!}$

Additionally, we define $\phi_0(f, x) := f_x(\emptyset)$ as the output of the model, if no feature is present. Notably, we have that if $f : \mathbb{C}^n \rightarrow A$, with $A = \mathbb{R}$ or \mathbb{C} , then $\phi \in A$. Additionally, if $f : \mathbb{C}^n \rightarrow \mathbb{C}$ we can split the output into its real and imaginary parts and explain them separately, since it holds that:

$$\begin{aligned} \phi_j(\mathcal{R}(f), x) &= \mathcal{R}(\phi_j(f, x)) \\ \phi_j(\mathcal{I}(f), x) &= \mathcal{I}(\phi_j(f, x)) \end{aligned} \quad (9)$$

5.2 Chain rule for DeepCSHAP

As pointed out before, DeepSHAP is not suitable to be used for complex-valued neural networks [21]. The reason is that the multiplier defined in Equation 4 is not suitable in complex-valued scenarios since complex-valued neural networks are usually not holomorphic (i.e. not complex differentiable) due to real output neurons or non-holomorphic activation functions. The quotient as defined in Equation 4 does not converge for $(x_j - \mathbb{E}(x_j)) \rightarrow 0$ and is thus not suitable for small perturbations.

A similar problem arises in the optimization of complex-valued neural networks, which is solved by using the Wirtinger derivatives for optimization instead of the complex derivative. The Wirtinger calculus motivates an alternative formulation of multipliers and a complex-valued chain rule that can be applied to complex-valued neural networks.

To define this complex-valued chain rule, we have to first define *partial contributions* of the real and imaginary part. This definition is motivated by the

following equation:

$$\phi_j(f, x) = \sum_{z' \subset x' \setminus j} G_{Mz'}(f_x(z' \cup j) - f_x(z')) \quad (10)$$

$$\begin{aligned} &= \sum_{z' \subset x' \setminus j} G_{Mz'}(f_x(z' \cup j) - f_x(z' \cup \mathcal{R}(j))) \\ &+ f_x(z' \cup \mathcal{R}(j)) - f_x(z') \end{aligned} \quad (11)$$

$$\begin{aligned} &= \sum_{z' \subset x' \setminus j} G_{Mz'}(f_x(z' \cup j) - f_x(z' \cup \mathcal{R}(j))) \\ &+ \sum_{z' \subset x' \setminus j} G_{Mz'}(f_x(z' \cup \mathcal{R}(j)) - f_x(z')) \end{aligned} \quad (12)$$

where $\mathcal{R}(j)$ means to have only the real part of the j -th feature present, while the imaginary part stays absent. We now define the *partial contributions* as the two summands of Equation 12:

$$\phi_{\mathcal{R}(j)}(f, x) = \sum_{z' \subset x' \setminus j} G_{Mz'}(f_x(z' \cup \mathcal{R}(j)) - f_x(z')) \quad (13)$$

$$\phi_{\mathcal{I}(j)}(f, x) = \sum_{z' \subset x' \setminus j} G_{Mz'}(f_x(z' \cup j) - f_x(z' \cup \mathcal{R}(j))) \quad (14)$$

Intuitively, the real partial contributions of a feature can be seen as the contributions of the real part of x , if the imaginary part of that feature is missing and the imaginary partial contribution as the contribution of the imaginary part, when the real part is never missing. These quantities themselves do not hold meaningful information but are important for the formulation of the chain rule later on since we can use them to define the *partial multipliers*:

$$m_{xf}^{\mathcal{R}(j)} = \frac{\phi_{\mathcal{R}(j)}(f, x)}{\mathcal{R}(x_j - \mathbb{E}(x_j))}; \quad m_{xf}^{\mathcal{I}(j)} = \frac{\phi_{\mathcal{I}(j)}(f, x)}{\mathcal{I}(x_j - \mathbb{E}(x_j))} \quad (15)$$

Inspired by Wirtinger calculus, we can now define the actual multipliers used for the chain rule:

$$m_{xf}^j = \frac{1}{2} \left(m_{xf}^{\mathcal{R}(j)} - i m_{xf}^{\mathcal{I}(j)} \right) \quad (16)$$

$$m_{\bar{x}f}^j = \frac{1}{2} \left(m_{xf}^{\mathcal{R}(j)} + i m_{xf}^{\mathcal{I}(j)} \right) \quad (17)$$

Before proceeding to the chain rule, we want to note two properties of the multipliers that will come in handy later on to reduce the computational load:

$$f : \mathbb{C} \rightarrow \mathbb{R} \Rightarrow m_{\bar{x}f}^j = \overline{m_{xf}^j} \quad (18)$$

$$f \text{ linear} \Rightarrow m_{xf}^j = \frac{\delta f}{\delta x_j} \text{ and } m_{\bar{x}f}^j = \frac{\delta f}{\delta \bar{x}_j} \quad (19)$$

where the derivative operators in the second property are meant as Wirtinger operators. Proofs for these properties as well as for the now following chain rule can be found in the supplementary material. The complex-valued chain rule for a concatenation $h = f \circ g$ with $g(y) = x \in \mathbb{C}^n$ is:

$$m_{yh}^k = \sum_{j=1}^n (m_{yg_j}^k m_{xf}^j + \overline{m_{yg_j}^k} m_{\overline{xf}}^j) \quad (20)$$

$$m_{\overline{y}h}^k = \sum_{j=1}^n (m_{\overline{y}g_j}^k m_{xf}^j + \overline{m_{\overline{y}g_j}^k} m_{\overline{xf}}^j) \quad (21)$$

Since we are interested in the contributions rather than the multipliers, we have to reconstruct them after the use of the chain rule:

$$\phi_{\mathcal{R}(k)}(h, x) = (m_{yh}^k + m_{\overline{y}h}^k) \mathcal{R}(x_k - \mathbb{E}(x_k)) \quad (22)$$

$$\phi_{\mathcal{I}(k)}(h, x) = (m_{yh}^k - m_{\overline{y}h}^k) i \mathcal{I}(x_k - \mathbb{E}(x_k)) \quad (23)$$

$$\phi_k(h, x) = \phi_{\mathcal{R}(k)}(h, x) + \phi_{\mathcal{I}(k)}(h, x) \quad (24)$$

We have summarized how to apply the chain rule to calculate the contributions of a concatenation of functions in Algorithm 1.

Note that by Equation 9 we can always assume the outer function f to be real-valued since if it is not, we can just calculate the contributions to the real and imaginary part separately by replacing f with $\mathcal{R}(f)$ and $\mathcal{I}(f)$. Thus, we can make use of Equation 18 to simplify the calculation of the chain rule.

For numerical stability, we adopt an adaptation from DeepSHAP: If the denominator in the fraction in the multipliers in Equation 15 is close to zero (in our case smaller than 10^{-6}), we replace it with the respective Wirtinger derivative.

Since the for-loop in Algorithm 1 can be vectorized and all operations can be defined as matrix multiplications, the algorithm can be efficiently computed on a GPU using deep learning frameworks (in our case: Pytorch). The contributions can then be computed in a single backward pass within milliseconds, see appendix for a runtime analysis.

5.3 MaxCSHAP

To apply the chain rule from subsection 5.2 we need to pre calculate the (partial) contributions $\phi_{\mathcal{R}}$ and $\phi_{\mathcal{I}}$ for every layer. [20] derives SHAP values for real-valued max pooling layers, however their algorithm is not suitable for complex-valued max pooling. Since the complex numbers are not ordered, max pooling is commonly done by ordering by the magnitude of the patch, thus for an image patch $\mathcal{X} = \{x_1, \dots, x_n\}$, we can define complex max pooling as

$$\mathbb{C}\text{maxpool} = \operatorname{argmax}_{x \in \mathcal{X}} |x| \quad (25)$$

In Algorithm 2 we define an algorithm to efficiently compute the contributions of a max pooling layer. For a presorted input (which can be accomplished in $O(n \log_2 n)$) the complexity of the algorithm is $O(n^2)$.

Algorithm 1

Complex-valued chain rule for contributions $\phi_k(h, x)$ of $h = f \circ g$:

Analytic. calc $\phi_{\mathcal{R}(k)}(g, y), \phi_{\mathcal{I}(k)}(g, y)$ $\triangleright *$

$$m_{yg}^{\mathcal{R}(k)} \leftarrow \frac{\phi_{\mathcal{R}(k)}(g, y)}{\mathcal{R}(y_k - \mathbb{E}(y_k))}$$

$$m_{yg}^{\mathcal{I}(k)} \leftarrow \frac{\phi_{\mathcal{I}(k)}(g, y)}{\mathcal{I}(y_k - \mathbb{E}(y_k))}$$

$$m_{yg}^k \leftarrow \frac{1}{2} \left(m_{yg}^{\mathcal{R}(k)} - i m_{yg}^{\mathcal{I}(k)} \right)$$

$$m_{\bar{y}g}^k \leftarrow \frac{1}{2} \left(m_{yg}^{\mathcal{R}(k)} + i m_{yg}^{\mathcal{I}(k)} \right)$$

for $j = 0$ **to** n **do**

Analytic. calc $\phi_{\mathcal{R}(j)}(f, x), \phi_{\mathcal{I}(j)}(f, x)$ $\triangleright *$

$$m_{xf}^{\mathcal{R}(j)} \leftarrow \frac{\phi_{\mathcal{R}(j)}(f, x)}{\mathcal{R}(x_j - \mathbb{E}(x_j))}$$

$$m_{xf}^{\mathcal{I}(j)} \leftarrow \frac{\phi_{\mathcal{I}(j)}(f, x)}{\mathcal{I}(x_j - \mathbb{E}(x_j))}$$

$$m_{xf}^j \leftarrow \frac{1}{2} \left(m_{xf}^{\mathcal{R}(j)} - i m_{xf}^{\mathcal{I}(j)} \right)$$

$$m_{\bar{x}f}^j \leftarrow \frac{1}{2} \left(m_{xf}^{\mathcal{R}(j)} + i m_{xf}^{\mathcal{I}(j)} \right)$$

end for

$$m_{yh}^k \leftarrow \sum_{j=1}^n (m_{ygj}^k m_{xf}^j + \overline{m_{ygj}^k} m_{\bar{x}f}^j)$$

$$m_{\bar{y}h}^k \leftarrow \sum_{j=1}^n (m_{\bar{y}gj}^k m_{xf}^j + \overline{m_{\bar{y}gj}^k} m_{\bar{x}f}^j)$$

$$\phi_{\mathcal{R}(k)}(h, x) \leftarrow (m_{yh}^k + m_{\bar{y}h}^k) \mathcal{R}(x_k - \mathbb{E}(x_k))$$

$$\phi_{\mathcal{I}(k)}(h, x) \leftarrow (m_{yh}^k - m_{\bar{y}h}^k) \mathcal{I}(x_k - \mathbb{E}(x_k))$$

$$\phi_k(h, x) \leftarrow \phi_{\mathcal{R}(k)}(h, x) + \phi_{\mathcal{I}(k)}(h, x)$$

* easy and fast for building blocks of CVNNs (e.g. linear layers, 1-to-1 activation etc.)

Algorithm 2

Contributions ϕ_k of \mathbb{C} max pooling:

Precomputed vector M $\triangleright *$

Input $X = (X_1, \dots, X_n)$

Reference $Y = (Y_1, \dots, Y_n)$

$$m \leftarrow \operatorname{argmax}_p(|X|, |Y|) \triangleright **$$

$$s \leftarrow \operatorname{argmax}(\operatorname{argmin}_p(|X|, |Y|))$$

for $k = 0$ **to** $n - 1$ **do**

$$m_x[k] \leftarrow \operatorname{argmin}(X[k], s)$$

$$m_y[k] \leftarrow \operatorname{argmin}(Y[k], s)$$

$$z_x \leftarrow \operatorname{sort}(m_x, \text{key} = |\cdot|)$$

$$z_y \leftarrow \operatorname{sort}(m_y, \text{key} = |\cdot|)$$

$$\phi_k \leftarrow \langle z_x, M \rangle - \langle z_y, M \rangle$$

end for

* constant vector M only depends on n and can be pre computed for every max pooling layer. It incorporates the weighting factors $G_{Mz'}$ from Equation 8.

** argmax_p denotes pointwise argmax

6 Evaluation

We evaluate our method DeepCSHAP in two experiments: An experiment on MNIST [16] as designed by Shrikumar et al. [23] and already presented for the evaluation of the real-valued DeepSHAP [20]. Additionally, we evaluate with a self designed experiment on a complex-valued PolSAR dataset [2]. Details on the training procedure for both experiments can be found in the supplementary material. Since no other explanation methods for complex-valued neural networks have been proposed, there is no competitive baseline, we could compare to. Comparing to an explanation algorithm for real-valued neural networks is not suitable either, since when comparing explanation methods between different models (e.g. a real-valued and a complex-valued to be able to apply the respective explanation method) we would not know, if a difference in our experiments has to be attributed to the difference in models, or the difference in explanation methods. Thus we treat the adaptations of gradient based methods in section 4 as baseline and compare our proposed DeepCSHAP against those.

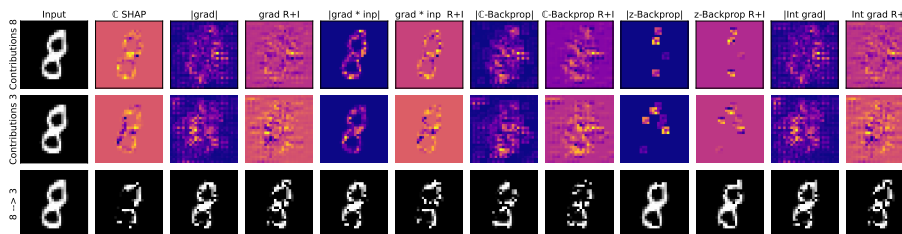


Fig. 3: Qualitative results for MNIST experiment. Explanation scores for output 8 and 3 are shown and the image after masking 20% of the most important pixels for both predictions. All images are normalized in itself, normalization over all methods is not suitable due to different orders of magnitude.

Additional to evaluating explanation quality, we also test our theoretical results from section 5 by verifying core properties of DeepCSHAP computationally.

6.1 MNIST experiment

We use a small complex-valued CNN with three blocks of \mathbb{C} convolutions, \mathbb{C} Relu activations and \mathbb{C} max pooling followed by a 2 layer MLP as a classifier on the MNIST dataset. The model obtains a 88% accuracy on the digit classification task on the test set of MNIST. We adopt the experimental setup as performed by [20, 23]: For a preset source class we randomly select an image from the test set and use the explanation methods to explain the source class output and the output for a fixed target class. We then identify up to 20% of the most important pixels for classifying the class correctly into the source class rather than into the target class by choosing the pixels with the highest explanation scores and remove these pixels by setting them to zero. We then input the modified image into the model and evaluate the change in log-odds compared to the initial input. A high score thus indicates the ability of the explanation algorithm to identify the most important features for a classification into a specific class. Qualitative results are visualized in Figure 3. All explanations are very blurry except DeepCSHAP and $|grad * input|$, which are the only methods whose explanations focus on the actual content of the image. This indicates that these methods assign contribution to the most important pixels. This is also visible in the quantitative results in Figure 4. There it shows that DeepCSHAP performs best on this task. This result is in line with the results in [20], where a similar result was shown for a real-valued neural network. While none of the gradient based methods is on par with DeepCSHAP, gradient times input and integrated gradients in the variant with the sum of real and imaginary parts show similarly good results. It is evident from these results, that the absolute value of the gradient leads to a worse performing explanation method, than the sum of real and imaginary part. The former performs very poorly for all methods except

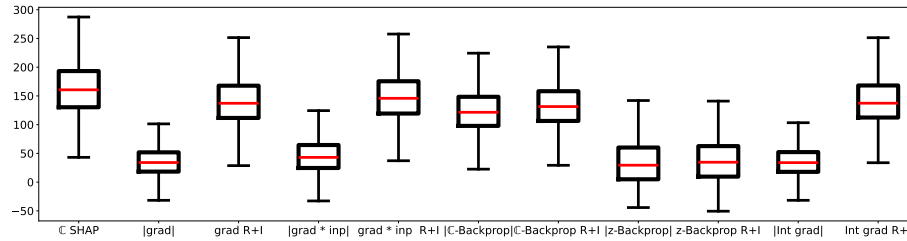


Fig. 4: Quantitative results on MNIST experiment. Change in log-odds after masking 20% of the most relevant features for classes 8 and 3 according to different explanation algorithms. The median is shown in red.

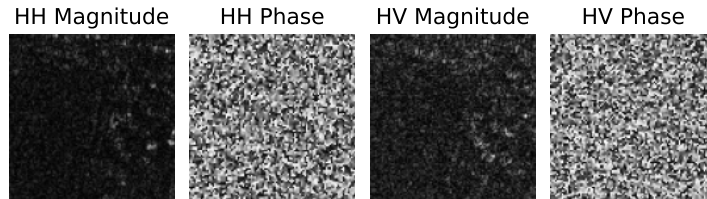


Fig. 5: Example image from the PolSAR S1SLC_CVDL dataset. Magnitude and Phase information of the complex-valued two channel (HH and HV) images are shown.

GuidedCBackpropagation. As for the two variants for Guided Backpropagation, the \mathbb{C} -ReLU version performs meaningfully better than the z -ReLU variant.

6.2 PolSAR experiment

For this experiments we trained a complex-valued version of the ResNet18 [10] with an Adam optimizer [14] on the S1SLC_CVDL [2] datasets. It consists of 276571 complex-valued PolSAR image patches of size 100×100 from three north American city areas. They are labeled with seven classes: Agriculture, Forest, High-Density Urban, High-Rise Urban, Low-Density Urban, Industrial and Water. Per image patch two complex-valued channels, HH and HV polarization, are available. As can be seen in Figure 5, these images are very noisy and thus a visual explanation is not feasible.

To still be able to evaluate explanation quality on this dataset, we designed an experiment on this task: We take two patches and input the four channels into the complex-valued neural network. As output we expect the classes of both patches, making this a multiclass classification problem. The trained model obtains an accuracy of 93% on this task (detailed results in the supp. material).

If we explain the output log-odds for the one of the two correct labels, we know that it should be explained by the two corresponding input channels and the other two input channels should have no or a negative influence on the prediction. We then measure to which extent this is fulfilled for a specific image

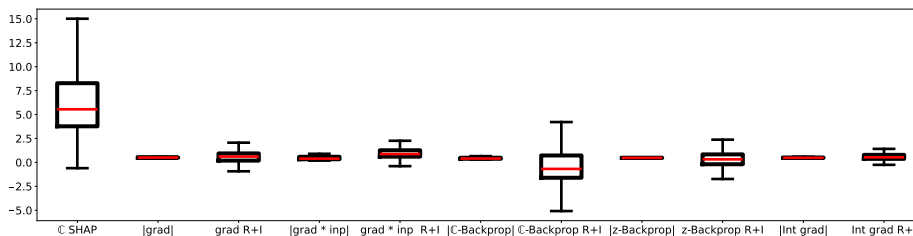


Fig. 6: Quantitative results for the PolSAR experiment. Fraction of calculated contributions from the correct channels versus all channels are visualized for all explanation methods introduced in this paper. For gradient based methods $|\cdot|$ denotes the absolute value of the respecting method, R+I denotes adding up real and imaginary part.

by this measure: Let X^1, X^2, Y^1, Y^2 be the four input channels from two patches from different classes. Let $\phi_k(f, Z)$ be the explanation by an explanation method of pixel $k \in \{1, \dots, n\}$ in channel Z . We then calculate:

$$\frac{\sum_{l=1}^2 \sum_{k=0}^n \phi_k(f, X^l)}{\sum_{l=1}^2 \sum_{k=0}^n \phi_k(f, X^l) + \sum_{l=1}^2 \sum_{k=0}^n \phi_k(f, Y^l)} \quad (26)$$

For strictly positive explanations, this measure is bounded at 1 and would signal that all important features are in the correct channels. For possibly negative values of signed explanation method (i.e. DeepCSHAP and the signed gradient variants) a value greater than 1 indicates that the incorrect channels contributed negatively to the final decision, which is desirable (since these channels show an image of a different class). Hence a score ≥ 1 is desirable.

Figure 6 shows that DeepCSHAP performs best on this task. All the gradient based methods perform relatively poorly. The results from the MNIST experiment are mostly confirmed, as the $\mathcal{R} + \mathcal{I}$ variants of gradient times input and integrated gradients perform best. Overall, the absolute value with median scores around 0.5, indicating that they marked the features of the incorrect channels to be equally important as the features of the correct channels. All variants of the Guided Backpropagation perform poorly, while the simple gradient explanation, gradient multiplied by input and integrated gradient show median scores around 1 when the real and imaginary parts are added.

6.3 Testing SHAP axioms

To verify our theoretical results from section 5 we test Missingness and Local Accuracy as two of the axioms of the SHAP framework.

To test Missingness, we report the percentage of missing inputs that are assigned a value other than 0 by DeepCSHAP. To test Local Accuracy, we report

	MNIST	S1SLC_CVDL
Local Accuracy Error	9.8×10^{-6}	3.5×10^{-3}
Average output	39.21	129.27
Missingness Error	0.0%	0.0%

Table 1: Validation of Local Accuracy and Missingness in DeepCSHAP. Local Accuracy error denotes the value from Equation 27. Average absolute value of the model output is reported to make the results for Local Accuracy comparable. Missingness error denotes the fraction of missing features that are assigned a non-zero contribution.

the average of the following equation over all outputs and the whole test set. Let X be an input image and f the prediction model:

$$\left| \left(\sum_{j=1}^n \phi_j(f, X) + \phi_0 \right) - f(X) \right| \quad (27)$$

As Table 1 shows, Missingness is always fulfilled. The (absolute) Local Accuracy Error of 9.8×10^{-6} and 3.5×10^{-3} (resulting in a relative error of 2.3×10^{-7} and 2.7×10^{-5}) on MNIST and S1SLC_CVDL respectively can be explained by the adaptations made for numeric stability.

7 Conclusion

In this paper we have introduced multiple explanation algorithms for complex-valued neural networks by adapting four gradient based explanation methods to the complex domain and by developing a complex-valued version of the well known DeepSHAP [20] explanation method, which we call DeepCSHAP. The major theoretical result to obtain the latter is the complex-valued chain rule for contributions as introduced in section 5. By providing these methods, we fill the gap of missing explanation methods for complex-valued neural networks, which are rising in popularity for applications with real- and complex-valued data types.

We analyze explanation quality on the real-valued MNIST dataset and the real world complex-valued PolSAR S1SLC_CVDL dataset. We show that our method DeepCSHAP outperforms the gradient based methods on both tasks.

Additionally, we have validated our theoretical results on these datasets. We show that the SHAP properties Local Accuracy and Missingness are fulfilled. This and the theoretical guarantees given by the theoretical foundation of Shapley values make this method suited to explain complex-valued neural networks.

As future work, we aim to adopt more explanation methods to the complex domain, such as LIME and kernelSHAP. Additionally, applying DeepCSHAP on different modalities will be interesting, especially modalities that are easily visually interpretable, such as MRI images to make use of the generated head maps, rather than quantitative results on the hard-to-understand PolSAR images.

References

1. Adadi, A., Berrada, M.: Peeking inside the black-box: a survey on explainable artificial intelligence (XAI). *IEEE Access* **6**, 52138–52160 (2018)
2. Asiyabi, R.M., Datcu, M., Anghel, A., Nies, H.: Complex-valued end-to-end deep network with coherency preservation for complex-valued SAR data reconstruction and classification. *IEEE Transactions on Geoscience and Remote Sensing* (2023)
3. Bach, S., Binder, A., Montavon, G., Klauschen, F., Müller, K.R., Samek, W.: On pixel-wise explanations for non-linear classifier decisions by layer-wise relevance propagation. *PloS one* **10**(7), e0130140 (2015)
4. Barrachina, J.A., Ren, C., Morisseau, C., Vieillard, G., Ovarlez, J.P.: Impact of PolSAR pre-processing and balancing methods on complex-valued neural networks segmentation tasks. *IEEE Open Journal of Signal Processing* **4**, 157–166 (2023)
5. Basse, J., Qian, L., Li, X.: A survey of complex-valued neural networks. *arXiv:2101.12249* (2021)
6. Chen, H., He, F., Lei, S., Tao, D.: Spectral complexity-scaled generalisation bound of complex-valued neural networks. *Artificial Intelligence* **322**, 103951 (2023)
7. Choi, H.S., Kim, J.H., Huh, J., Kim, A., Ha, J.W., Lee, K.: Phase-aware speech enhancement with deep complex U-Net. In: *ICLR* (2018)
8. Cole, E., Cheng, J., Pauly, J., Vasanawala, S.: Analysis of deep complex-valued convolutional neural networks for MRI reconstruction and phase-focused applications. *Magnetic Resonance in Medicine* **86**(2), 1093–1109 (2021)
9. Eilers, F., Jiang, X.: Building blocks for a complex-valued transformer architecture. In: *IEEE International Conference on Acoustics, Speech and Signal Processing (ICASSP)* (2023)
10. He, K., Zhang, X., Ren, S., Sun, J.: Deep residual learning for image recognition. In: *IEEE Conference on Computer Vision and Pattern Recognition*. pp. 770–778 (2016)
11. Hirose, A.: *Complex-Valued Neural Networks: Theories and Applications*. World Scientific (2003)
12. Hu, Y., Liu, Y., Lv, S., Xing, M., Zhang, S., Fu, Y., Wu, J., Zhang, B., Xie, L.: DCCRN: Deep complex convolution recurrent network for phase-aware speech enhancement. In: *INTERSPEECH* (2020)
13. Kindermans, P.J., Schütt, K., Müller, K.R., Dähne, S.: Investigating the influence of noise and distractors on the interpretation of neural networks. *arXiv:1611.07270* (2016)
14. Kingma, D.P., Ba, J.: Adam: A method for stochastic optimization. In: *3rd International Conference on Learning Representations ICLR* (2015)
15. Ko, M., Panchal, U.K., Andrade-Loarca, H., Mendez-Vazquez, A.: Coshnet: A hybrid complex valued neural network using shearlets. *arXiv:2208.06882* (2022)
16. LeCun, Y.: The MNIST database of handwritten digits. <http://yann.lecun.com/exdb/mnist/> (1998)
17. Lee, C., Hasegawa, H., Gao, S.: Complex-valued neural networks: A comprehensive survey. *IEEE/CAA Journal of Automatica Sinica* **9**(8), 1406–1426 (2022)
18. Li, X., Sun, Q., Li, L., Liu, X., Liu, H., Jiao, L., Liu, F.: SSCV-GANs: Semi-supervised complex-valued GANs for PolSAR image classification. *IEEE Access* **8**, 146560–146576 (2020)
19. Lin, Q.H., Niu, Y.W., Sui, J., Zhao, W.D., Zhuo, C., Calhoun, V.D.: SSPNet: An interpretable 3D-CNN for classification of schizophrenia using phase maps of resting-state complex-valued fMRI data. *Medical Image Analysis* **79**, 102430 (2022)

20. Lundberg, S.M., Lee, S.I.: A unified approach to interpreting model predictions. *Advances in Neural Information Processing Systems* **30** (2017)
21. Mayer, K.S., Müller, C., Soares, J.A., de Castro, F.C.C., Arantes, D.S.: Deep phase-transmittance RBF neural network for beamforming with multiple users. *IEEE Wireless Communications Letters* **11**(7), 1498–1502 (2022)
22. Ribeiro, M.T., Singh, S., Guestrin, C.: "Why should I trust you?" explaining the predictions of any classifier. In: 22nd ACM SIGKDD International Conference on Knowledge Discovery and Data Mining. pp. 1135–1144 (2016)
23. Shrikumar, A., Greenside, P., Kundaje, A.: Learning important features through propagating activation differences. In: International Conference on Machine Learning. pp. 3145–3153. PMLR (2017)
24. Simonyan, K., Vedaldi, A., Zisserman, A.: Deep inside convolutional networks: Visualising image classification models and saliency maps. In: 2nd International Conference on Learning Representations (ICLR) (2014)
25. Springenberg, J.T., Dosovitskiy, A., Brox, T., Riedmiller, M.A.: Striving for simplicity: The all convolutional net. In: 3rd International Conference on Learning Representations (ICLR) (2015)
26. Štrumbelj, E., Kononenko, I.: Explaining prediction models and individual predictions with feature contributions. *Knowledge and Information Systems* **41**, 647–665 (2014)
27. Sundararajan, M., Taly, A., Yan, Q.: Gradients of counterfactuals. arXiv:1611.02639 (2016)
28. Tan, Z.H., Xie, Y., Jiang, Y., Zhou, Z.H.: Real-valued backpropagation is unsuitable for complex-valued neural networks. *Advances in Neural Information Processing Systems* **35**, 34052–34063 (2022)
29. Trabelsi, C., Bilaniuk, O., Zhang, Y., Serdyuk, D., Subramanian, S., Santos, J.F., Mehri, S., Rostamzadeh, N., Bengio, Y., Pal, C.J.: Deep complex networks. In: 6th International Conference on Learning Representations (ICLR) (2018)
30. Vasudeva, B., Deora, P., Bhattacharya, S., Pradhan, P.M.: Compressed sensing MRI reconstruction with Co-VeGAN: Complex-valued generative adversarial network. In: WACV. pp. 1779–1788 (2022)
31. Yang, M., Ma, M.Q., Li, D., Tsai, Y.H.H., Salakhutdinov, R.: Complex transformer: A framework for modeling complex-valued sequence. In: IEEE International Conference on Acoustics, Speech and Signal Processing (ICASSP). pp. 4232–4236 (2020)
32. Yin, D., Luo, C., Xiong, Z., Zeng, W.: Phasen: A phase-and-harmonics-aware speech enhancement network. In: AAAI Conference on Artificial Intelligence. vol. 34, pp. 9458–9465 (2020)
33. Zhang, H., Gu, M., Jiang, X., Thompson, J., Cai, H., Paesani, S., Santagati, R., Laing, A., Zhang, Y., Yung, M., et al.: An optical neural chip for implementing complex-valued neural network. *Nature Communications* **12**(1), 457 (2021)

DeepCSHAP: Utilizing Shapley Values to Explain Deep Complex-Valued Neural Networks

Supplementary Material

8 Proof of properties of complex-valued multipliers

We want to prove the following properties for complex-valued multipliers as mentioned in the main paper in Equations 18 - 19:

$$f : \mathbb{C} \rightarrow \mathbb{R} \Rightarrow m_{\bar{x}f}^j = \overline{m_{xf}^j} \quad (28)$$

$$f \text{ linear} \Rightarrow m_{xf}^j = \frac{\delta f}{\delta x_j} \text{ and } m_{\bar{x}f}^j = \frac{\delta f}{\delta \bar{x}_j} \quad (29)$$

Equation 28 follows from the fact that if $f : \mathbb{C} \rightarrow \mathbb{R}$, then $\phi_j(\mathcal{R}(f), x)$ and $\phi_j(\mathcal{I}(f), x)$ are real-valued and then also $m_{xf}^{\mathcal{R}(j)}$ and $m_{xf}^{\mathcal{I}(j)}$. Thus it holds that:

$$m_{\bar{x}f}^j = \frac{1}{2} \left(m_{xf}^{\mathcal{R}(j)} + i m_{xf}^{\mathcal{I}(j)} \right) \quad (30)$$

$$= \frac{1}{2} \left(m_{xf}^{\mathcal{R}(j)} - i m_{xf}^{\mathcal{I}(j)} \right) \quad (31)$$

$$= \overline{m_{xf}^j} \quad (32)$$

To prove Equation 29 let $f(x) := Ax$ with $A \in \mathbb{C}^{1 \times n}$ (for multidimensional output, we analyze each output separately and thus every row of A separately), then with Equation 13 / 14 and $\Delta x := x - \mathbb{E}(x)$, we get:

$$\phi_{\mathcal{R}(j)}(f, x) = A_j \mathcal{R}(\Delta x_j) \text{ and} \quad (33)$$

$$\phi_{\mathcal{I}(j)}(f, x) = i A_j \mathcal{I}(\Delta x_j) \quad (34)$$

and thus:

$$m_{xf}^{\mathcal{R}(j)} = \frac{A_j \mathcal{R}(\Delta x_j)}{\mathcal{R}(\Delta x_j)} = A_j \text{ and} \quad (35)$$

$$m_{xf}^{\mathcal{I}(j)} = \frac{i A_j \mathcal{I}(\Delta x_j)}{\mathcal{I}(\Delta x_j)} = i A_j \quad (36)$$

It then follows:

$$m_{xf}^j = \frac{1}{2} (A_j - i^2 A_j) = A_j = \frac{\delta f}{\delta x_j} \quad (37)$$

$$m_{\bar{x}f}^j = \frac{1}{2} (A_j + i^2 A_j) = 0 = \frac{\delta f}{\delta \bar{x}_j} \quad (38)$$

□

9 Proof of chain rule

To prove the chain rule for complex-valued multipliers (Equations 20 and 21 in the main paper), we have to show:

$$\sum_{k \leq m} \phi_k(h, y) = h(y) - \phi_0 \quad (39)$$

when applying the chain rule for complex-valued multipliers. For an easier notation let $\Delta z = z - \mathbb{E}(z)$. Then it holds:

$$\sum_{k \leq m} \phi_k(h, y) \quad (40)$$

$$= \sum_{k \leq m} (\phi_{\mathcal{R}(k)}(h, y) + \phi_{\mathcal{I}(k)}(h, y)) \quad (41)$$

$$= \sum_{k \leq m} m_{yh}^{\mathcal{R}(k)} \mathcal{R}(\Delta y_k) + m_{yh}^{\mathcal{I}(k)} \mathcal{I}(\Delta y_k) \quad (42)$$

$$= \sum_{k \leq m} m_{yh}^{\mathcal{R}(k)} \mathcal{R}(\Delta y_k) + m_{yh}^{\mathcal{I}(k)} \mathcal{I}(\Delta y_k) \quad (43)$$

$$= \sum_{k \leq m} (m_{\bar{y}h}^k + m_{yh}^k) \mathcal{R}(\Delta y_k) + (m_{yh}^k - m_{\bar{y}h}^k) i \mathcal{I}(\Delta y_k) \quad (44)$$

$$= \sum_{k \leq m} \sum_{j \leq n} ((m_{\bar{y}g_j}^k m_{x_f}^j + \overline{m_{\bar{y}g_j}^k} m_{\bar{x}_f}^j) \quad (45)$$

$$+ (m_{yg_j}^k m_{x_f}^j + \overline{m_{yg_j}^k} m_{\bar{x}_f}^j)) \mathcal{R}(\Delta y_k) \quad (46)$$

$$+ ((m_{\bar{y}g_j}^k m_{x_f}^j + \overline{m_{\bar{y}g_j}^k} m_{\bar{x}_f}^j) \quad (47)$$

$$- (m_{\bar{y}g_j}^k m_{x_f}^j + \overline{m_{\bar{y}g_j}^k} m_{\bar{x}_f}^j)) i \mathcal{I}(\Delta y_k) \quad (48)$$

$$= \sum_{k \leq m} \sum_{j \leq n} ((m_{\bar{y}g_j}^{\mathcal{R}(k)} m_{x_f}^j + \overline{m_{\bar{y}g_j}^{\mathcal{R}(k)}} m_{\bar{x}_f}^j) \mathcal{R}(\Delta y_k) \quad (49)$$

$$+ (m_{yg_j}^{\mathcal{I}(k)} m_{x_f}^j + \overline{m_{yg_j}^{\mathcal{I}(k)}} m_{\bar{x}_f}^j) (-i) i \mathcal{I}(\Delta y_k)) \quad (50)$$

$$= \sum_{j \leq n} (m_{x_f}^j (\Delta x_j) + m_{\bar{x}_f}^j (\overline{\Delta x_j})) \quad (51)$$

$$= \sum_{j \leq n} ((m_{x_f}^j + m_{\bar{x}_f}^j) \mathcal{R}(\Delta x_j) + (m_{x_f}^j - m_{\bar{x}_f}^j) \mathcal{I}(\Delta x_j)) \quad (52)$$

$$= \sum_{j \leq n} \phi_{\mathcal{R}(j)}(f, x) + \phi_{\mathcal{I}(j)}(f, x) \quad (53)$$

$$= \sum_{j \leq n} \phi_j(f, x) \quad (54)$$

$$= f(x) - \phi_0 \quad (55)$$

$$= h(y) - \phi_0 \quad (56)$$

□

	Agriculture	Forest	High Density Urban	Buildings	Low Density Urban	Industrial	Water
Precision	0.999	0.999	0.999	0.997	0.999	0.999	0.999
Recall	0.941	0.946	0.680	0.722	0.650	0.863	0.999

Table 2: Per class precision and recall of the complex-valued ResNet18 trained on the SISLC_CVDL dataset.

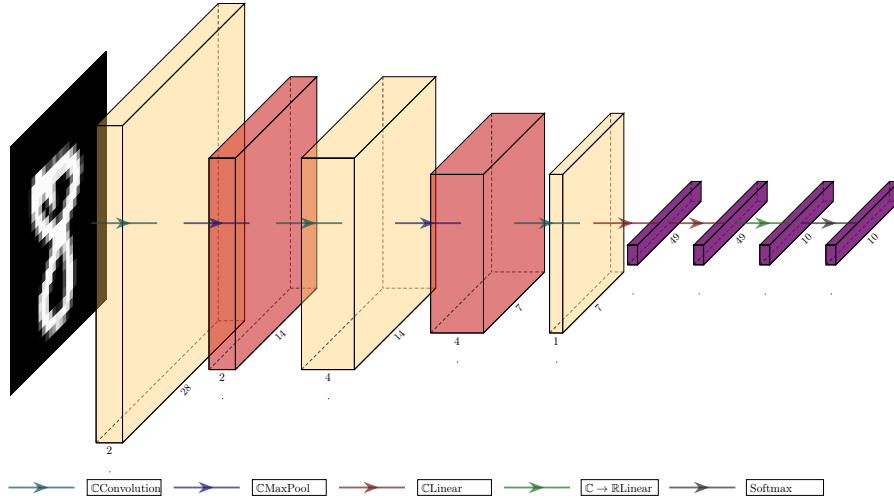


Fig. 7: CConvolutional model designed for the MNIST dataset task.

10 Details on training and results – PolSAR

The experimental setup is explained in detail subsection 6.2. We used a complex-valued version of the ResNet18 [10] with four input channels and 7 outputs classes, where the ground truth label has one or two classes, making this a multiclass classification problem. We trained the model with an Adam [14] optimizer in pytorch. The model adaptation to the complex domain was made, as suggested by Trabelsi et al. [29]. The training was performed with the following hyperparameters:

- Learning rate: 0.001
- Epochs: 20
- Loss: binary cross entropy
- Adam betas: 0.9, 0.999

The test accuracy of the trained model is 0.93, precision and recall for the individual classes can be seen in Table 2.

11 Details on training and results – MNIST

We use a small complex-valued CNN with three blocks of \mathbb{C} convolutions, \mathbb{C} Relu activations and \mathbb{C} max pooling followed by a 2 layer MLP as a classifier on the MNIST dataset as can be seen in Figure 7. We train with an Adam [14] optimizer in pytorch. The model was build from building blocks as suggested by Trabelsi et al. [29] with max pooling layers as described in subsection 5.3. The training was performed with the following hyperparameters:

- Learning rate: 0.001
- Epochs: 20
- Loss: cross entropy
- Adam betas: 0.9, 0.999

The test accuracy of the trained model is 0.88.

12 Runtime analysis of explanation methods

	DeepCSHAP	Grad	Grad*Input	C-Backprop	z-Backprop	int. Grad
MNIST	132	5.0/4.7	4.7/4.7	5.3/5.3	5.2/5.4	22.6/22.6
S1SLC_CVDL	380	57.2/57.8	59.4/59.7	64.1/63.8	63.3/63.3	302/302

Table 3: Runtime of different explanation methods on both datasets in milliseconds. For gradient based methods (all but DeepCSHAP) the first number shows the result for the version when using the absolute value, the second number when using $\mathcal{R} + \mathcal{I}$.

For both experiments from section 6 we performed a runtime analysis for all explanation methods presented in section 5 and section 4. Results can be seen in Table 3. As expected, all the gradient based methods are very fast. Just the integrated gradient method is significantly slower than the other methods, which is expected, since for the the integration the gradient has to be calculated for multiple inputs. We use 5 integrands which corresponds with the slow down factor of ~ 5 . As can be observed, DeepCSHAP is the slowest of all the explanation methods. It is however still relatively fast, being able to explain ~ 8 images per second on MNIST and ~ 3 images per second on the S1SLC_CVDL PolSAR dataset.